CONSTRUCTION OF 3-D MODELS OF NUCLEI IN A HEPATIC HISTOPATHLOGICAL SPECIMEN

T. Kojima*, M. Takahashi* and M. Nakano**

* Shibaura Institute of Technology, Saitama, 337-8570, Japan
** Chiba Medical Center, Chiba, 260-8606, Japan

mtaka@sic.shibaura-it.ac.jp

Abstract: Histopathologic images observed using an optical microscope usually have blur. It is desirable to remove the blur and to construct a three-dimensional (3-D) model of a histopathological specimen so that the diagnosis can be more accurate. It would also be possible to measure the 3-D nuclear density if 3-D nuclei models could be constructed. Thus, we attempted to remove blur in the images captured using an optical microscope and construct 3-D models of nuclei. As a method to remove blur, we examined the applicability of blind deconvolution (BD). It was experimentally confirmed that the blur in a 3-D image of a hepatic histopathological specimen could be reduced by employing such a BD. We also improved the constraint conditions for BD. These new constraint conditions reduced the error and eliminated unusual patterns in the Point Spread Function (PSF) and blur; thereby, the resultant 3-D object image was improved. The 3-D object image was displayed using volume rendering by ray casting. These results show that 3-D nuclei models featuring fine structures can be constructed and displayed.

Introduction

Histopathologic diagnosis is a diagnosis method to observe microscopic images of sliced tissue. It is said to be the most accurate method of diagnosing diseases such as cancer. However, it depends on the subjectivity of the pathologist. Therefore, a problem arises in that different diagnoses may be arrived at for similar specimens.

To solve this problem, image analysis can be employed to identify quantitative features that would be useful for the diagnosis. For example, we built a system to calculate nuclear densities, which are very important in differential diagnosis of early well-differentiated hepatocellular carcinoma [1].

However, there were two problems that had to be overcome.

(i) The difference in the thickness of a specimen affects the nuclear density. A nuclear density is originally three-dimensional (3-D) information (the number per unit volume). However, nuclear density is usually calculated as two-dimensional (2-D) information (the number per unit area). (see Figure 1) A 3-D nuclear density would be measurable if accurate 3-D nuclei models could be constructed. However, the second problem means that it is difficult to construct such 3-D models.

(ii) Microscopic images deteriorate depending on the thickness of a specimen. This problem is caused by the effect of the out-of-focus area. Pathologists have to make diagnoses from images including blur. (Figure 2)

These problems can be solved by constructing a 3-D model of the specimen. In particular, blind deconvolution [2] (BD) is a practical way to remove blur and to construct a 3-D image because it does not require a point spread function (PSF) to be measured. However, as far as we know, there are almost no reports concerning its application to the histopathologic specimens such as liver. In addition, there is a possibility that BD can not be applied to histopathologic specimens including objects such as nuclei that have large absorptions, because BD assumes that the absorption is not large.

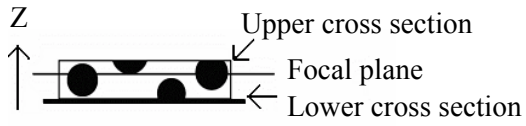

Figure 1: Change in 2-D nuclear density depending on thickness (Z coordinate). Black circles indicate nuclei. The 2-D nuclear density changes depending on the plane being observed (Z coordinate).

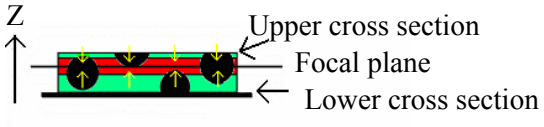

Figure 2: Effect of the depth of focus (DOF). Black circles indicate nuclei. DOF is shown in the red area. If the thickness is larger than DOF/2, the area outside the DOF (shown in green) affects the image, resulting in a blurry image.

The purposes of our research are as follows.

(a) Verification of the applicability of BD to histopathologic specimens.
(b) Improvement of the conventional BD algorithm according to 3-D incoherent imagery theory.

ISSN: 1727-1983 © 2005 IFMBE

(c) Construction of 3-D models of nuclei for estimating the 3-D nuclear density.

Moreover, we take into account that an optical microscope will be used to capture the images because pathologists usually use optical microscopes for their histopathologic diagnoses. Although there are other microscopes that have higher resolutions, e.g., the confocal laser microscope, these devices are very expensive and are rarely used in normal diagnosis. Thus, we believed that a method that uses an optical microscope would be used by more pathologists.

Materials and Methods

[A] Outline of the method

(i) Image capture: Microscopic images of hepatic histopathologic specimens (Argentation stained) are captured while changing the focus position to obtain the observed 3-D image.

(ii) Object image estimation using BD: The object 3-D image is estimated by applying 3-D BD to the observed 3-D image.

(iii) Construction of 3-D nuclei models: 3-D volume data are generated using the object 3-D image, and the 3-D models of the nuclei are constructed using volume rendering.

[B] Image capture

Figure 3 shows the system for capturing images. The system is composed of a PC and a microscope (E-400, NIKON) in which a CCD camera (SPOT INSIGHT IN1120, DIAGNOSTIC INSTRUMENTS, 1600x1200 pixels) and a stage (OptiScan ES103, Prior) are installed. Microscopic images were captured while moving the computer-controlled stage downward (-Z direction) by 0.1 μm. This procedure was repeated (Figure 4), and a set of 2-D images having different focus positions was obtained for the observed 3-D image. The magnification factor of the objective lens was 100 (NA: 1.3).

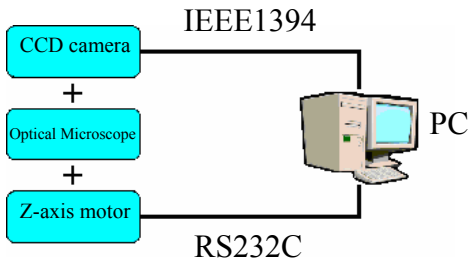

Figure 3: Configuration of image-capture system

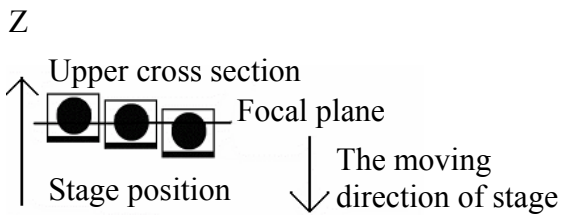

Figure 4: Consecutive scan.

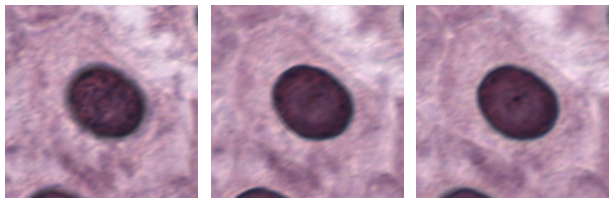

Figure 5: Examples of captured images. The Z positions of the images differ by 1μm.

[C] Object image estimation using blind deconvolution

[C-i] What is blind deconvolution ?

Equation 1 shows the model of the observed image in the 2-D case. The observed image *g(x,y)* is expressed as a convolution of the object image *f(x,y)* and a point spread function (PSF) *h(x,y)*. Blur in the observed image occurs if the PSF has blur that might have been due to defocusing, etc.

$$g(x,y) = f(x,y) * h(x,y) \quad (1)$$

BD estimates both the unknown *f(x,y)* and unknown *h(x,y)* at a same time by using the observed image *g(x,y)* and information such as a priori knowledge. The blur which originates from the PSF can be removed by estimating the object image *f(x,y)*.

An advantage of BD over the non-blind deconvolution method is that it does not require measurement of the PSF. In fact, measuring the PSF is a difficult and time-consuming process. Furthermore, PSFs might be different if the specimens or the image capture devices such as the objective lenses are different. Pathologists need not be concerned about such differences when using BD. Thus, a method using BD should be more practical than a non-blind one.

[C-ii] Algorithm of blind deconvolution

We thought that the algorithm proposed by Holmes et al. [2] would be a promising BD algorithm to apply to 3-D data. The algorithm is outlined below. Please refer to the papers [2], [3] and [4] for more details.

To make a histopathologic diagnosis, the pathologist observes a TLB (Transmitted Light Brightfield) image showing the intensity of light transmitted through the specimen. In this case, it is appropriate to estimate the absorption coefficient of the histopathologic specimen as an object image because the specimen absorbs light [5][6]. Therefore, we used the model shown in Figure 6.

Figure 7 and Figure 8 show the estimation procedure for the object image $\lambda(x,y,z)$ and the PSF *h(x,y,z)*.

$$\mu_n(x,y,z) = B - \mu_P(x,y,z) = B - \lambda(x,y,z) * h(x,y,z) \quad (2)$$

μ_n: Observed image, B: Background light intensity,
μ_p: Absorption quantity in observed image,
h: PSF, λ: Object image (Absorption coefficient of histopathologic specimen)

Figure 6: A model for BD

ISSN: 1727-1983 © 2005 IFMBE

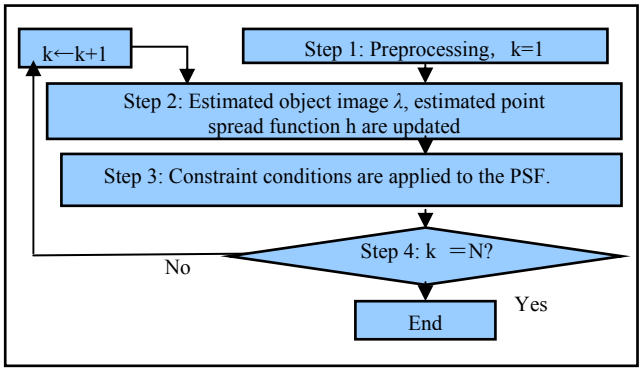

Figure 7: Flowchart of BD algorithm [2]. N is the number of repetitions.

In Step 2, the object image λ and PSF h are updated according to the equations below, where * means convolution.

$$\lambda_{k+1} = \left[\frac{\mu_p(x,y,z)}{\lambda_k(x,y,z) * h_k(x,y,z)} * h_k(-x,-y,-z) \right] \cdot \lambda_k(x,y,z) \quad (3)$$

$$h_{k+1} = \left[\frac{\mu_p(x,y,z)}{\lambda_k(x,y,z) * h_k(x,y,z)} * \lambda_k(-x,-y,-z) \right] \cdot h_k(x,y,z) \quad (4)$$

The constraint conditions applied to the PSF in Step 3 are as follows.

(a) The values in the PSF must be 0 outside a biconical area defined by the NA of the objective lens.
(b) All the values in the PSF must be equal to or more than 0.
(c) The values in the optical transfer function (OTF), which is a discrete Fourier transform of the PSF, must be 0 outside the bandlimit.

[C-iii] Improvement of blind deconvolution

As is described before, the values in the OTF outside the bandlimit are set to 0. This bandlimit is calculated as follows in the conventional BD.

Figure 9 shows the bandlimit regions of the conventional and improved BDs. In the conventional method shown as yellow and green areas, the radial bandlimit (bandlimit for the ρ direction) is defined as $2NA/\lambda$, which is the reciprocal of the resolution to the radial direction. The axial bandlimit (bandlimit for η direction) is defined as 1/2DOF, which is the reciprocal of twice the depth of focus (DOF).

According to 3-D image formation theory [7][8], however, the axial bandlimit depends on the spatial frequency to the radial direction, and the bandlimit region is defined as the region in which the formula shown in Figure 8 holds [9]. This bandlimit region is also shown in Figure 9 as the red and yellow areas. Thus, the yellow area is the area used by both the conventional and improved methods. The improved BD used constraint conditions on the OTF corresponding to the yellow and red areas in Figure 9.

F: F number,
λ: wavelength,

$$1.0 - \left(\lambda\rho F + \frac{2|\eta|F}{\rho} \right)^2 > 0 \quad (5)$$

(u,v,w) : Coordinates in spatial frequency region

$$\rho = \left(u^2 + v^2\right)^{0.5}, \quad \eta = w$$

Figure 8: Improved BD conditions for the spatial frequency in the OTF. If the spatial frequency does not satisfy these conditions, the OTF value for that spatial frequency is set to 0.

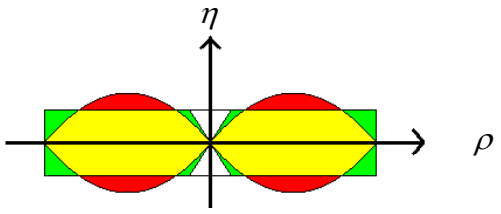

Figure 9: Comparison of OTF bandlimit regions: Green areas are used in the conventional method. Red areas are used in the improved method. Yellow areas are used by both methods.

[D] Construction of 3-D models of nuclei

(i) The object image is converted into 3-D field data after BD has been performed.
(ii) The 3-D field data is displayed using volume rendering by ray casting.

Results

A hepatic histopathologic specimen (Argentation stained) was used in the experiment. Two-hundred transmitted light brightfield images were captured using x100 objective lens (NA:1.3) while moving the computer-controlled stage downward (-Z) by 0.1μm. A partial 3-D image (300 x 300 x 200 voxels) including the nuclei was cut from the resultant 3-D image and used. The dimensions of one voxel were 0.073 μm x 0.073 μm x 0.1 μm.

ISSN: 1727-1983 © 2005 IFMBE

[E] Results of blind deconvolution

Figure 10 shows XY, XZ and YZ cross-section images at the center of the 3-D observed image. Figure 11 shows XY, XZ and YZ cross-section images of the 3-D object image after the improved BD had been applied. The BD had 1000 repetitions. The values of 3-D image were inverted and normalized so that nuclei looked dark and the values did not exceed 256. Comparing Figure 10 and Figure 11, we can see that the blur in the area outside the tissue is reduced in Figure 11. This improvement is the effect of BD. However, there is still blur outside the tissue where the absorption coefficient is very small. The remaining blur is especially large near the nucleus, which has a large absorption coefficient. Further improvements will be necessary to remove most of the blur from areas that include objects having large absorption coefficients.

[F] Comparison of conventional and improved methods

Figure 12 shows an XY, XZ and YZ cross-section image of the 3-D object image after the conventional BD had been applied. The blur in the red ellipse is reduced in the XZ and YZ cross-section image obtained by using the improved BD (Figure 11). This comparison demonstrates the effect of the improved BD.

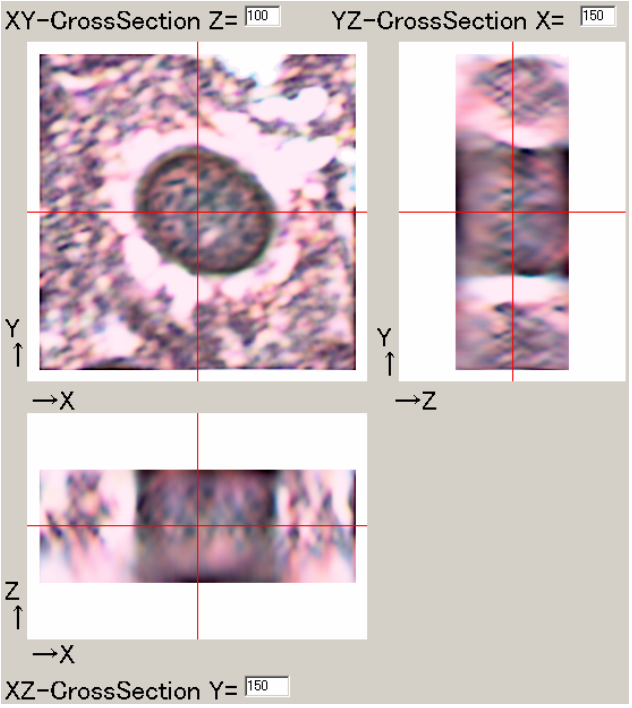

Figure 11: XY, XZ and YZ cross-section images of the 3-D object image after improved BD

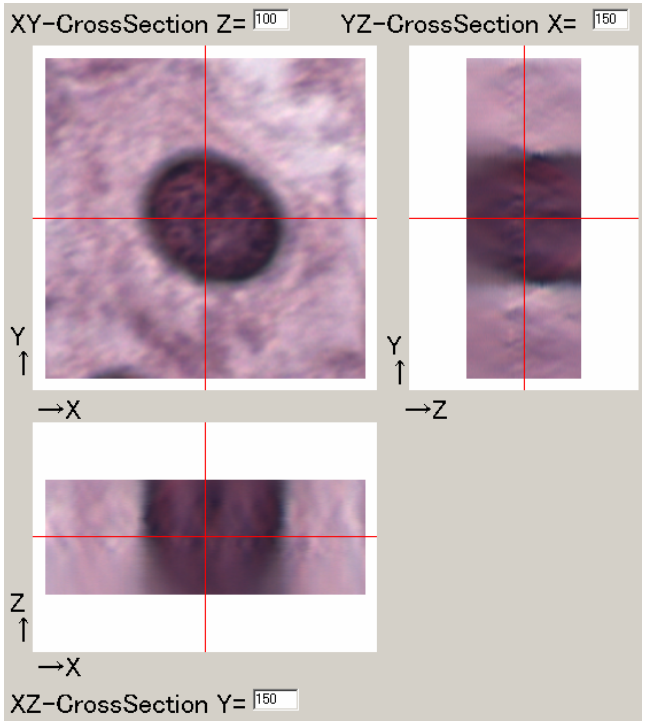

Figure 10: XY, XZ and YZ cross-section images of the observed 3-D image at the center of the 3-D image

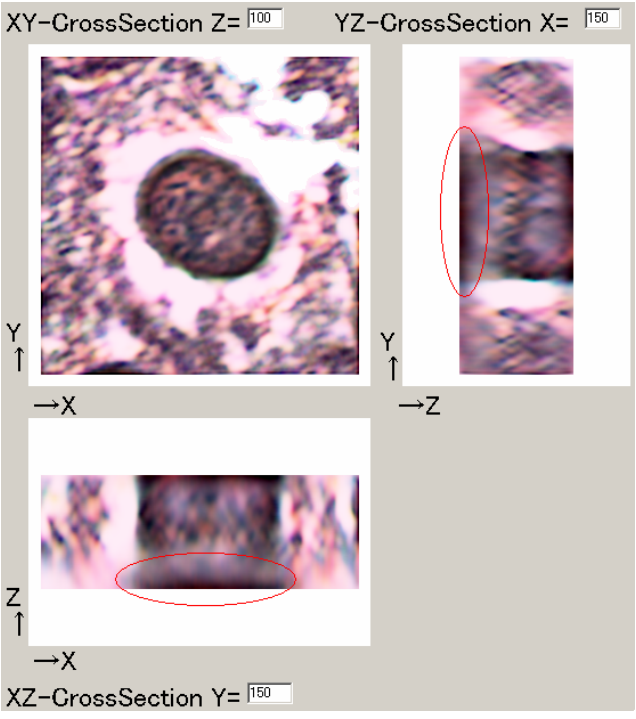

Figure 12: XY, XZ and YZ cross-section image of the 3-D object image after conventional BD

ISSN: 1727-1983 © 2005 IFMBE

Figure 13 shows the residual errors (RE) per one voxel for the conventional (blue) and improved (red) methods, and Figure 14 shows the difference between the two errors. RE is calculated by subtracting the absorption in the observed image from the convolution of the estimated object image (absorption coefficient) and estimated PSF. These figures show that the RE of the improved method is always smaller than the RE of the conventional method.

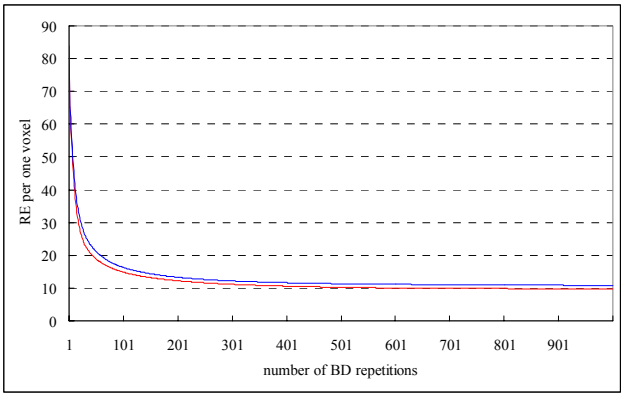

Figure 13: Residual errors per one voxel for conventional (blue) and improved (red) methods

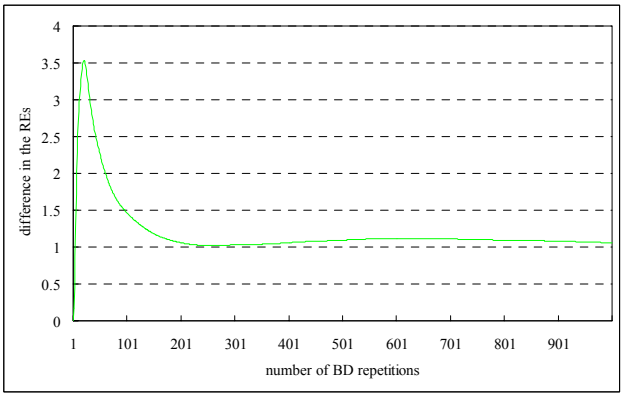

Figure 14: The difference in residual errors per one voxel between conventional and improved methods

Figures 15 and 16 show the XY, XZ and YZ cross-section images of PSF after applying the conventional and improved BDs. The conventional BD causes an unusual periodic pattern to appear in the upper and lower areas of the PSF shown in Figure 15. Such an unusual pattern does not appear in the image created with the improved BD (Figure 16).

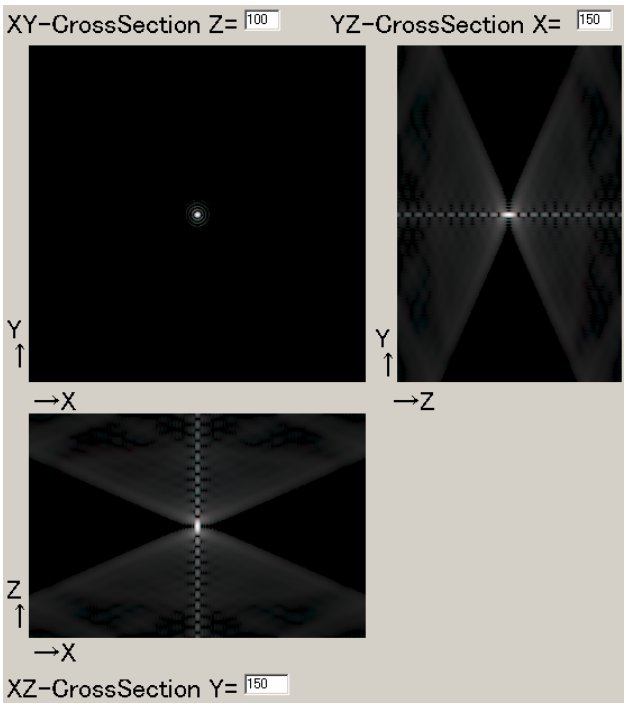

Figure 15: XY, XZ and YZ cross-section image of PSF after conventional BD

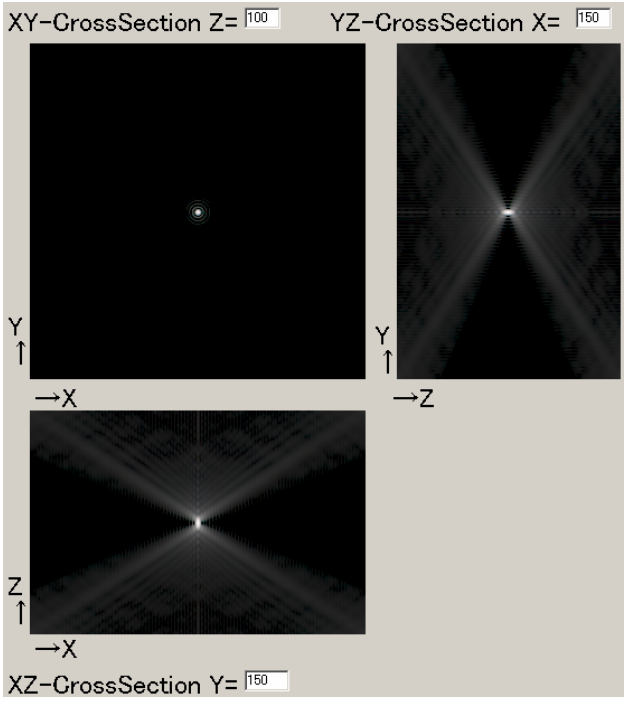

Figure 16: XY, XZ and YZ cross-section image of PSF after improved BD

[G] Construction of 3-D models of nuclei

3-D models of nuclei were constructed by using the 3-D object image obtained from the improved BD. R-channel was used for constructing the 3-D models because the result using R-channel was better than those obtained using other channnels.

ISSN: 1727-1983 © 2005 IFMBE

Figure 17 and Figure 18 are top views of the 3-D model. Fine 3-D structures, such as in the nuclei, can be observed, and the overall 3-D structure can be easily grasped by the viewer.

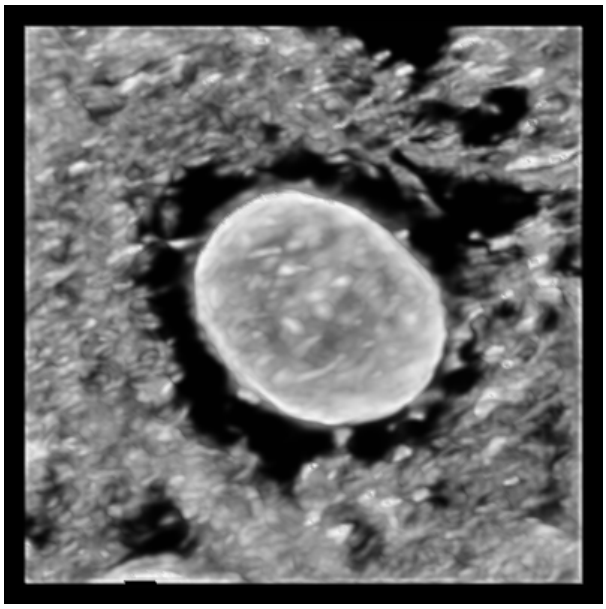

Figure 17: 3-D model of the nucleus (top view)

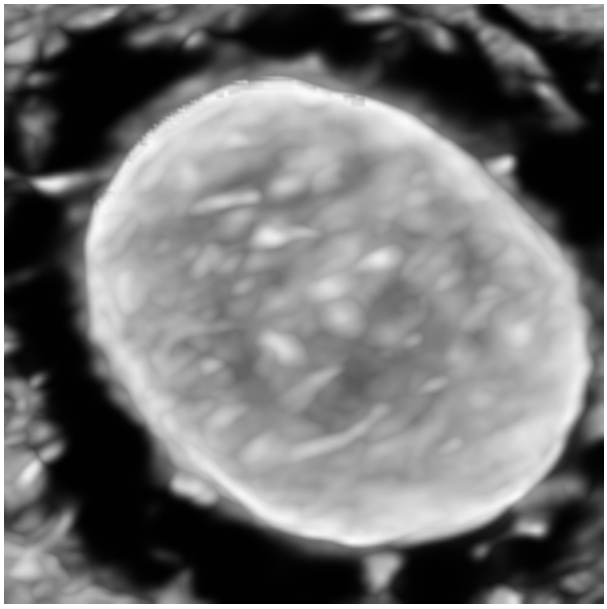

Figure 18: 3-D model of the nucleus (top view, magnified image)

Discussion

The results of our study are summarized as follows.

(i) Blur in the 3-D image of a histopathologic specimen was reduced by applying a 3-D blind deconvolution (BD).

(ii) The improved BD was better than the conventional one at reducing error and blur.

(iii) 3-D nuclei models having fine structures could be constructed.

These results were obtained using images captured by an ordinary optical microscope. Hence, the method can be used by many pathologists who do not have access to expensive types of microscopes.

However, some degree of blur remained in the estimated 3-D object image, especially near nuclei having large absorption coefficients. The use of more constraints that are peculiar to histopathologic specimens would be a way to remove most of the resultant blur.

Acknowledgements

This research was partially supported by the Ministry of Education, Science, Sports and Culture, Grant-in-Aid for Scientific Research (C), 16500302, 2005.

References

[1] TAKAHASHI M. and NAKANO M. (2004): 'Histo-pathlogic Diagnosis Support System for Early Well-Differentiated HCC', IAP2004 – The XXV Cong. Of the Intl. Academy of Pathology, Australia, 2004, A20-5

[2] HOLMES, T. J. and O'CONNOR, N. J. (2000): 'Blind Deconvolution of 3D Transmitted Light Brightfield Micrographs', *J. Microsc*., **200**, pp. 114-127

[3] HOLMES, T. J. (1992): 'Blind Deconvolution of Quantum－Limited Incoherent Imagery', *J. Opt. Soc. Am. A*., **9**(7), pp. 1052-1061

[4] HOLMES, T. J., S.BHATTACHARYYA, J. A. COOPER, D. HANZEL, V. KRISHNAMURTHI, W. LIN, B. ROYSAM, D. SZROWSKI, and J. N. TURNER (1995): 'Light microscopic images reconstructed by maximum likelihood deconvolution', in JAMES B. PAWLEY. (Ed):'Handbook of biological confocal microscopy', 2nd ed. (Plenum Press, New York), pp. 389-402

[5] MACIAS-GARZA, F., DILLER, K. R., BOVIK. A. C., AGGARWAL. S. J., and AGGARWAL. J. K. (1989): 'Improvement in the Resolution of Three-Dimensional Data Sets Collected Using Optical Serial Sectioning', *J. Microsc*., **153**, pp. 205-221

[6] WILLIS, B., TURENER J. N., COLLINS D. N., ROYSAM B., and HOLMES T. J. (1993): 'Development in Three Dimensional Stereo Brightfield Microscopy', *Microscopic Research and Technique*, **24**, pp. 437-451

[7] STREIBL. N. (1984): 'Depth Transfer by an Imaging System', *Opt. Act*., **31**, pp. 1233-1241

[8] STREIBL. N. (1985): 'Three-Dimensional Imaging by a Microscope', *J. Opt. Soc. Am. A*. **2**, pp. 121-127

[9] TSURUTA T. (1993): 'Image formation of three dimensional objects', in TSURUTA T. (Ed): 'The third: pencil of ray', (New technology communications, Tokyo), pp. 391-409. (*in Japanese*)

ISSN: 1727-1983 © 2005 IFMBE